PAPER • OPEN ACCESS

Characterising the frequency response of impedance changes during evoked physiological activity in the rat brain

To cite this article: Mayo Faulkner *et al* 2018 *Physiol. Meas.* **39** 034007

IOP Publishing Physiol. Meas. 39 (2018) 034007 (9pp) https://doi.org/10.1088/1361-6579/aab01f

Physiological Measurement

IPEM Institute of Physics and Engineering in Medicine

OPEN ACCESS

PAPER

Characterising the frequency response of impedance changes during evoked physiological activity in the rat brain

Mayo Faulkner, Sana Hannan, Kirill Aristovich, James Avery and David Holder

University College London, London WC1E 6BT, United Kingdom

E-mail: mayo.faulkner@ucl.ac.uk

RECEIVED
4 December 2017

REVISED
13 February 2018

ACCEPTED FOR PUBLICATION
16 February 2018

PUBLISHED
2 April 2018

Keywords: electrical impedance tomography, fast neural EIT, evoked potentials

Abstract

Objective: Electrical impedance tomography (EIT) can image impedance changes associated with evoked physiological activity in the cerebral cortex using an array of epicortical electrodes. An impedance change is observed as the externally applied current, normally confined to the extracellular space is admitted into the conducting intracellular space during neuronal depolarisation. The response is largest at DC and decreases at higher frequencies due to capacitative transfer of current across the membrane. Biophysical modelling has shown that this effect becomes significant above 100 Hz. Recordings at DC, however, are contaminated by physiological endogenous evoked potentials. By moving to 1.7 kHz, images of somatosensory evoked responses have been produced down to 2 mm with a resolution of 2 ms and 200 μm. Hardware limitations have so far restricted impedance measurements to frequencies <2 kHz. The purpose of this work was to establish the optimal frequency for extending EIT to image throughout the brain and to characterise the response at frequencies >2 kHz using improved hardware. *Approach*: Impedance changes were recorded during forepaw somatosensory stimulation in both cerebral cortex and the VPL nucleus of the thalamus in anaesthetised rats using applied currents of 1 kHz to 10 kHz. *Main results*: In the cortex, impedance changed by -0.04 ± 0.02 % at 1 kHz, reached a peak of -0.13 ± 0.05 % at 1475 Hz and decreased to -0.05 ± 0.02 % at 10 kHz. At these frequencies, changes in the thalamus were -0.26 ± 0.1%, -0.4 ± 0.15 % and -0.08 ± 0.03 % respectively. The signal-to-noise ratio was also highest at 1475 Hz with values of -29.5 ± 8 and -31.6 ± 10 recorded from the cortex and thalamus respectively. *Signficance*: This indicates that the optimal frequency for imaging cortical and thalamic evoked activity using fast neural EIT is 1475 Hz.

1. Introduction

1.1. Background

Electrical impedance tomography (EIT) can be used to detect impedance changes associated with the depolarisation of neurons during evoked physiological activity (Klivington and Galambos 1967, Velluti *et al* 1968, Oh *et al* 2011). Under resting conditions, applied current is restricted to the extracellular space due to the capacitive membrane of neurons. When activity is evoked, ion channels in the receptive neural tissue open and provide a low resistance pathway into the intracellular space through which current can additionally travel (Cole and Curtis 1939) manifesting as a voltage change on the recording electrodes.

The impedance response is highly dependent on the frequency of current used and a number of models have been developed to predict its frequency characteristics. Liston *et al* (2012) developed a biophysical model based on cable theory for a single unmyelinated peripheral nerve axon which was then extended to characterise cortical tissue. Their model predicted that the impedance change monotonically decreases from around 1% when direct current (DC) is applied to 0.01% at 10 kHz. An alternative modelling approach approximated the cortex as a suspension of spherical spheres with passive cell membranes (Cole 1928, Vongerichten 2014). This predicted a drop in the impedance of 0.1% between DC and 2 kHz (Vongerichten *et al* 2016). More recently Tarotin *et al* (2017) have established a model based on the Hodgkin and Huxley equations (Hodgkin and Huxley 1952) which takes into account both the passive and active properties of ion channels. Their model of interacting unmyeli-

nated nerve fibres similarly shows a monotonic decrease in the impedance change from DC to higher frequencies (Tarotin *et al* 2017).

EIT imaging experiments using DC have been conducted during median nerve stimulation with electrodes placed on the cortex of an anaesthetised rabbit (Holder *et al* 1996) and in humans subject to a visual stimulus while recording with scalp electrodes (Gilad and Holder 2009). In both studies, however, a sufficient signal-to-noise ratio (SNR) for imaging could not be achieved. While the impedance signal itself may be larger at low frequency currents, inherent problems exist with their application. At these frequencies, the recorded voltages comprise the impedance change in addition to an artefact due to the evoked activity. The influence of the latter can be alleviated by subtraction of a separately recorded evoked potential when DC current is applied (Gilad and Holder 2009) or in the case of low AC frequencies by implementing phase randomisation averaging (Aristovich *et al* 2015). Complete removal of this artefact, however, can only be achieved by moving to a frequency band where the EP is no longer present, >1 kHz (Aristovich *et al* 2015). Measurements at low frequencies are also contaminated by spontaneous brain activity, EEG, the power spectrum of which falls by a factor greater than 1000 between DC and 1 kHz (Oh *et al* 2011).

In light of the problems at frequencies below 1 kHz, the emphasis has shifted toward obtaining measurements at higher frequencies. Vongerichten (2014) characterised the impedance response in the cortex during forepaw somatosensory stimulation up to 2 kHz and found that the largest SNR could be obtained when injecting between 1.5 kHz to 2 kHz. Using a carrier frequency of 1725 Hz, Aristovich *et al* (2016b) were successfully able to obtain the first EIT images of activity in the cortex of an anaesthetised rat.

The Vongerichten (2014) study was limited to frequencies below 2 kHz due to the anti-aliasing filter in the EEG amplifier used. There is an interest in characterising the impedance response at higher frequencies to identify whether a larger SNR can be achieved and in view of using a multi-frequency parallel EIT system. Parallel EIT involves the simultaneous injection of current at differing frequencies and is envisaged for use in applications such as epilepsy where averaging can not be conducted (Dowrick *et al* 2015). Epileptic activity occurs on millisecond timescales (Vongerichten *et al* 2016) and to achieve sufficient resolution for imaging, injecting frequencies must be separated by at least 1 kHz. This will necessitate the injection of current at frequencies greater than 2 kHz and an understanding of the impedance response at these higher frequencies is essential.

Currently, EIT imaging of fast neural activity has only been demonstrated in the cortex; however, it has the potential to image throughout the brain (Aristovich *et al* 2016b). The sensitivity of EIT is known to decay with distance from the electrodes (Alessandrini and Scapin 2017) and maximising the signal from deep structures will be crucial if EIT is to image activity below the cortex. Somatosensory evoked potentials are an ideal paradigm for deep imaging as their reproducibility is such that one can take advantage of averaging to increase the signal strength. Prior to converging in the cortex, afferents from the medial lemniscal and spinothalamic pathways terminate in the ventral posterolateral (VPL) thalamic nucleus (Paxinos 2014) and sizeable evoked potentials have been measured from this structure (Aguilar *et al* 2008, Alonso-Calvino *et al* 2016). As well as the cortex, the work presented has thus also focused on finding the optimal frequency to maximise the signal occurring in the VPL.

1.2. Purpose

The purpose of this work was to conduct a comprehensive frequency sweep to characterise the spectrum of the impedance change occurring in the cortex and the thalamus during forepaw evoked activity. The questions to be answered were,

(i) What are the characteristics of the impedance signal across frequency in the cerebral cortex and thalamus?
(ii) How do the impedance responses compare to known electrophysiology and biophysical models?
(iii) What are the implications for fast neural EIT applications in the brain?

1.3. Experimental design

Experiments were conducted in anaesthetised rats. Somatosensory activity was evoked through stimulation of the contralateral forepaw at 2 Hz. To characterise the cortical response, a 57-channel electrode array was placed on the surface of the cortex. When measuring thalamic activity, in addition to the cortical array, a depth electrode was placed in the ventral posterolateral (VPL) nucleus in the thalamus. The depth electrodes were only used to record voltages. For both the cortical and thalamic case two injection pairs were chosen from the electrodes on the cortical array. Cortical injection pairs were chosen to maximise sensitivity around the electrode that exhibited the largest evoked potential. The injection pairs used to record thalamic activity were chosen on an ad hoc basis based on the pairs that yielded a thalamic signal on the depth contacts. It was found that in order to detect a thalamic impedance change, a standing voltage exceeding 4 mV on the depth contacts was necessary. On the whole this could be achieved through injection of current between the electrode located nearest the depth probe and that located furthest away from the probe.

The impedance response was characterised using frequencies ranging from 1 kHz to 10 kHz. The lower frequency bound was chosen such that even when implementing a 500 Hz bandwith, the majority of the EEG noise could be eliminated from recordings. The early indication was that the maximum SNR lay below 3 kHz. Recordings were, therefore, taken at smaller frequency intervals between 1 kHz and 3 kHz. At each frequency impedance measurements using two different injection pairs were obtained. Despite recording from all 57 and 16 electrodes for the cortical and thalamic case respectively, for each injection pair, only measurements from the single recording electrode that exhibited that largest impedance response was chosen to characterise the response.

The actiCHamp EEG amplifier (Brainproducts GmbH, Germany) used for recordings has a hardware anti-aliasing filter of 7.5 kHz. To account for any attenuation in the amplitude of the signal due to this filter, its response in the frequency range of interest was characterised across a resistor phantom. The impedance changes recorded were normalised by the inverse of this response. This ensured that the observed impedance spectrum was solely due to physiological changes.

An estimate of the phase angle at all frequencies was computed by determination of the phase difference between the injecting and recording channels. Even at the largest frequency considered, 10 kHz, the largest phase angle was 7°. For all frequencies, therefore, the modulus of the impedance change was interpreted to be representative of the resistive component.

2. Methods

2.1. Animal preparation

Six female Sprague-Dawley rats weighing between 300–400 g were used in experiments. Anaesthesia was induced in a perspex box using a mixture of isoflurane, O_2 and air. Once anaesthetised a tracheal intubation was performed and anaesthesia maintained with isoflurane (2–2.5%) and a 50/50% mixture of O_2 and N_2O. Depth of anaesthesia was monitored by assessment of the pedal withdrawal and corneal reflexes. Cannulation of the right femoral vessels was then undertaken. The rat was then fixed within ear bars in a stereotaxic frame (Narishige International Ltd, UK) and mechanical ventilation using the SAV03 ventilator (Vetronic Services Ltd, UK) commenced. The rats head was shaved and the scalp incised and the left temporal muscle cauterized using a bipolar cauterization system (Malis CMC 2, Codman, USA) and reflected off the skull until the zygomatic arch came into view. A craniotomy was performed on the left hemisphere using a veterinary bone drill (Ideal Micro Drill, US). It extended from just rostral of lambda down to 4 mm rostral of bregma and laterally along the zygomatic arch. The bone flap was lifted and the dura incised in a crescent shape using a dura hook and micro-scissors and reflected over the mid-line to protect the superior sagittal sinus. Throughout the craniotomy and upon removal of the skull and dura, the brain was frequently irrigated with warm (38 °C) 0.9% NaCl solution. A 57 contact electrode array was then placed on the exposed cortex. In the rats where the thalamic response was characterised, an additional 16-channel depth electrode was placed through a hole in the array into the VPL (ML = 3–3.5 mm , AP = 2.5–3 mm , DV = 5–6 mm). A 1.5 cm diameter Ag/AgCl reference electrode was placed under the skin at the back of the neck and two silver needle electrodes were placed in the right forepaw for stimulation. Upon completion of surgery, a bolus of 60 mg kg^{-1} of 1% w v^{-1} α-chloralose in saline was administered intravenously and then maintained at 20 mg kg^{-1}. During this period, the rat was gradually weaned off the isoflurane and N_2O. After switching off the isoflurane and N_2O, one hour was allowed before commencing recordings to ensure they were mostly eliminated from the body. Any excess NaCl solution was removed from the brain prior to recording. Throughout the experiment ECG, end tidal $C0_2$, respiratory rate, SPO_2, mean arterial blood pressure and exhaled gas concentration and were all monitored using the Lightning Vetronics monitor (Vetronic Services Ltd, UK) and kept within the recommended physiological range. The core body temperature of the rat was controlled using a homeothermic heating unit comprising a heating blanket and a rectal probe that provided temperature feedback to the system (Harvard Apparatus, UK).

2.2. EIT hardware and data collection

Data were collected using the ScouseTom EIT system (Avery *et al* 2017) with the actiCHamp EEG amplifier. The electrode array was fabricated using a 12.5 μm sheet of stainless steel sandwiched between two layers of silicone. A laser was used to expose fifty-seven 0.6 mm diameter contacts that had a centre-to-centre spacing of 1.2 mm. The exposed electrode contacts were coated with platinum black prior to placement on the brain in order to reduce contact impedance. When recording the thalamic responses, a single shank depth electrode (Neuronexus, US) containing sixteen 30 μm diameter contacts spanning a length of 1500 μm was also implanted. Data collected on the depth contacts were passed through a unity gain headstage amplifier (Plexon, TX, USA). The contralateral forepaw was stimulated using a Neurolog NL800A (Digimeter, UK) isolated current stimulator. The forepaw was stimulated at a frequency of 2 Hz using pulses that were 500 μs in duration with a peak amplitude of 10 mA.

A complete frequency sweep constituted two consecutive single-channel impedance measurements at a total of 28 different frequencies that ranged from 1025 Hz to 9975 Hz. In each sweep, the frequency addressing order

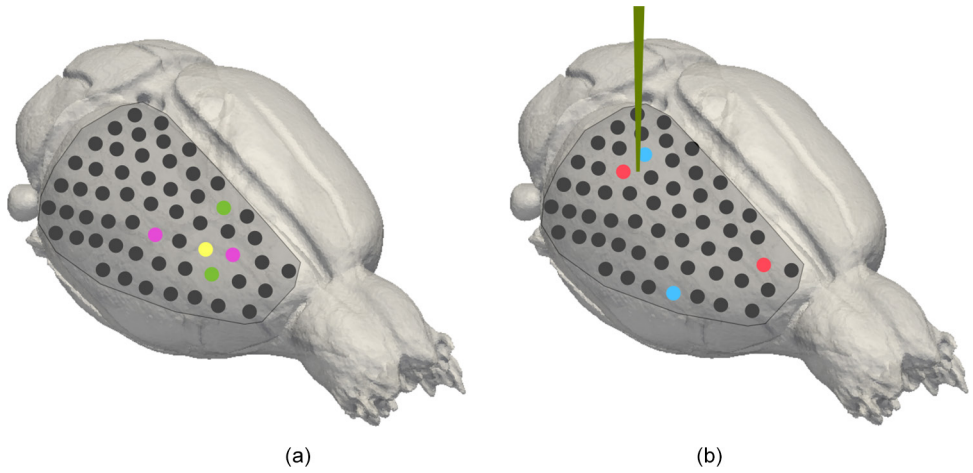

Figure 1. Experimental setup in the cortical (a) and thalamic case (b). In the cortex, injection pairs were chosen around the electrode that exhibited the largest evoked potential (yellow electrode in (a)) and are shown in green and pink. Examples of thalamic injection pairs are shown in (b) in blue and red.

was randomised. When characterising the cortical response, the electrode pairs were chosen in the vicinity of the electrode that exhibited the largest evoked response (figure 1(a)). For the thalamic case, two injection pairs that yielded a large impedance change in the VPL were chosen (figure 1(b)). Current was injected between a single pair of electrodes for 30 s and the amplitude of injected current was 50 μA and 200 μA when measuring from the cortex and thalamus respectively. In each rat, three comprehensive frequency sweeps were performed. The cortical response was characterised in $N = 3$ rats and similarly the thalamic response in $N = 3$ different subjects. Simultaneous characterisation of the cortical and thalamic response in a single rat was not undertaken.

2.3. Data processing

Data from single injection pairs at each carrier frequency were processed individually. A $\pm$200 Hz bandpass filter (5th order butterworth) was applied around the carrier frequency and demodulated using the Hilbert transform. The data were then segmented into sixty 500 ms epochs that spanned from 250 ms pre-stimulus to 250 ms post-stimulus. The mean of the baseline (200 ms to 50 ms pre-stimulus) was subtracted from each epoch in order to express the signal as a voltage change. As this voltage change is representative of the change in impedance within the object, from hereon in it will be referred to as an impedance change. The epochs were then averaged together yielding a mean impedance change. The SNR of the signal was computed by dividing the mean impedance change by the standard deviation of the baseline. Any attenuation of the signal due to the intrinsic response of the actiCHamp amplifier was accounted for by multiplying the impedance change and SNR at each frequency by the inverse of the amplifiers frequency response.

For each injection pair, the electrode that exhibited the largest impedance change was chosen for further analysis. For the cortical case, one channel out of the fifty-seven on the electrode array was selected. In the case of the thalamus, one out of the sixteen electrodes on the depth probe was chosen. When considering two injection pairs, three repeats within subjects and data from three subjects, this resulted in 18 impedance traces at all frequencies for both the cortical and thalamic response.

To characterise the response across frequency, the maximum negative amplitude and SNR, as well as the latency at which these occurred, were determined individually for each channel. These values were established at all frequencies and were averaged together.

Frequencies that exhibited a significant SNR were determined by comparing the mean SNR at each frequency to the mean SNR obtained across all frequencies. At each frequency a one sided t-test was performed with the significance level set to $\alpha = 0.01$.

To determine if a significant difference in latency was present across frequencies, the peak mean latency at each frequency was compared to the mean latency across all frequencies. In this case a two sided t-test was performed with the significance level set to $\alpha = 0.01$.

3. Results

3.1. Cortical impedance response

In the cerebral cortex, the peak impedance change was -4.6 ± 3 μV (-0.04 ± 0.02%) at 1025 Hz (figure 2(a)). This increased to a maximum of -15.4 ± 3 μV (-0.13 ± 0.05%) at 1475 Hz. By 3725 Hz it decreased to -2.7 ± 1 μV (-0.026 ± 0.01%). It remained fairly constant at frequencies above this. At 9975 Hz an impedance

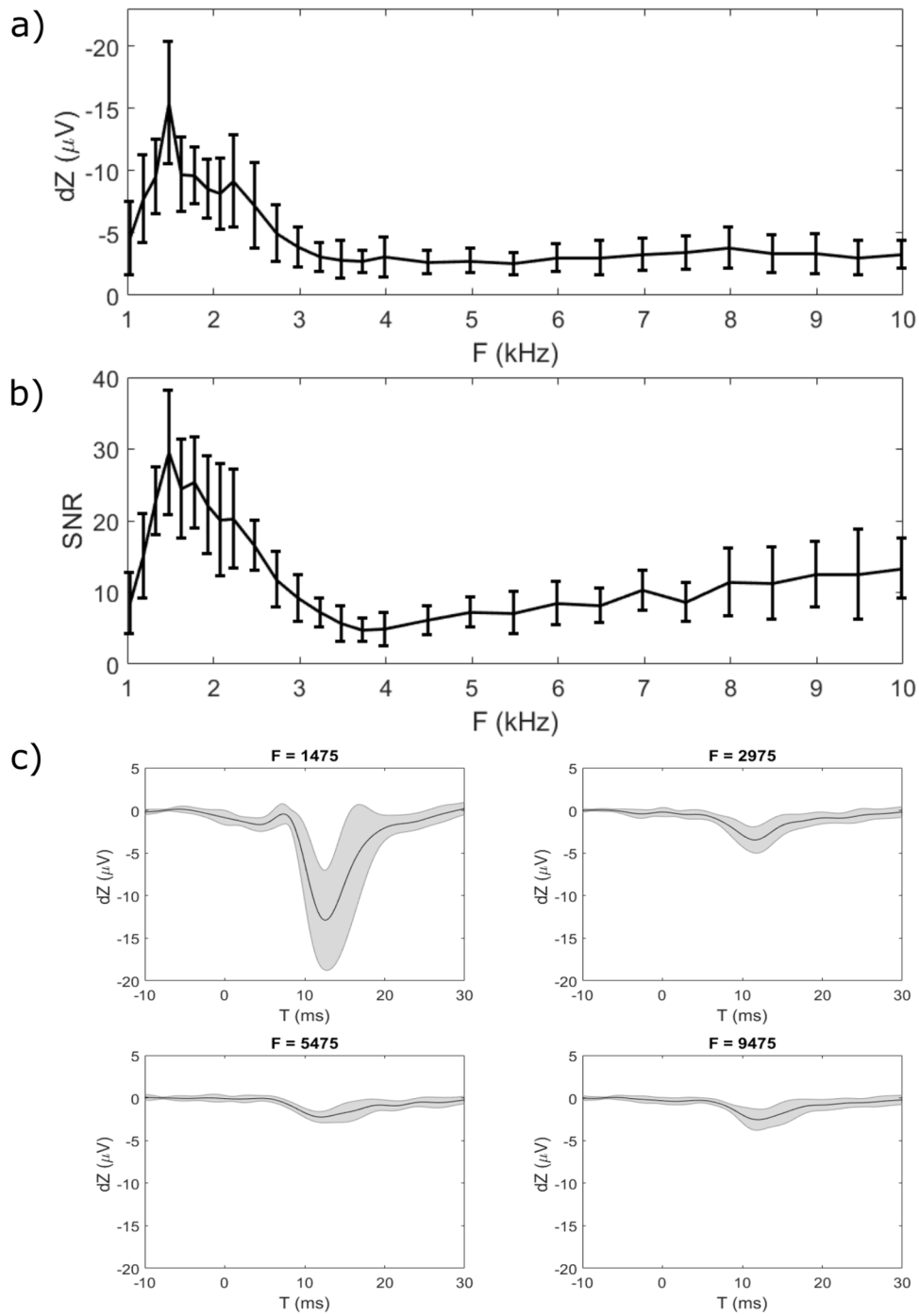

Figure 2. Frequency response of impedance change during somatosensory forepaw stimulation in cortex. (a) Peak impedance change with varying carrier frequency. (b) SNR with varying carrier frequency. (c) Examples of impedance traces at 1475 Hz, 2975 Hz, 5475 Hz and 9475 Hz. All values are given as (mean ± S.D.).

change of -3.3 ± 1 μV ($-0.05 \pm 0.02\%$) was observed. The mean latency of the peak response at 1475 Hz and 5475 Hz was 12.7 ± 1.3 ms and 12.4 ± 1.7 ms after stimulation. A significant difference in the peak latency was not observed at any frequency ($p < 0.01$).

The SNR increased from 8.5 ± 4 at 1025 Hz to a maximum of 29.5 ± 8 at 1475 Hz. It then decreased away reaching a minimum value of 4.8 ± 2 at 3725 Hz (figure 2(b)). The SNR at frequencies between 1325 Hz–2225 Hz exhibited a significant response ($p < 0.01$).

3.2. Thalamic impedance response

In the thalamus the peak impedance change was -10.1 ± 3 μV ($-0.26 \pm 0.1\%$) at 1025 Hz (figure 3(a)). It increased to a maximum amplitude of -16.9 ± 4 μV ($-0.40 \pm 0.15\%$) at 1475 Hz. By 2975 Hz it decreased to -4.9 ± 1 μV ($-0.08 \pm 0.04\%$). At 9975 Hz the impedance change had the lowest magnitude of -2.2 ± 0.7 μV ($-0.08 \pm 0.03\%$). The mean latency of the peak response at 1475 Hz was 7.9 ± 1.4 ms after stimulation.

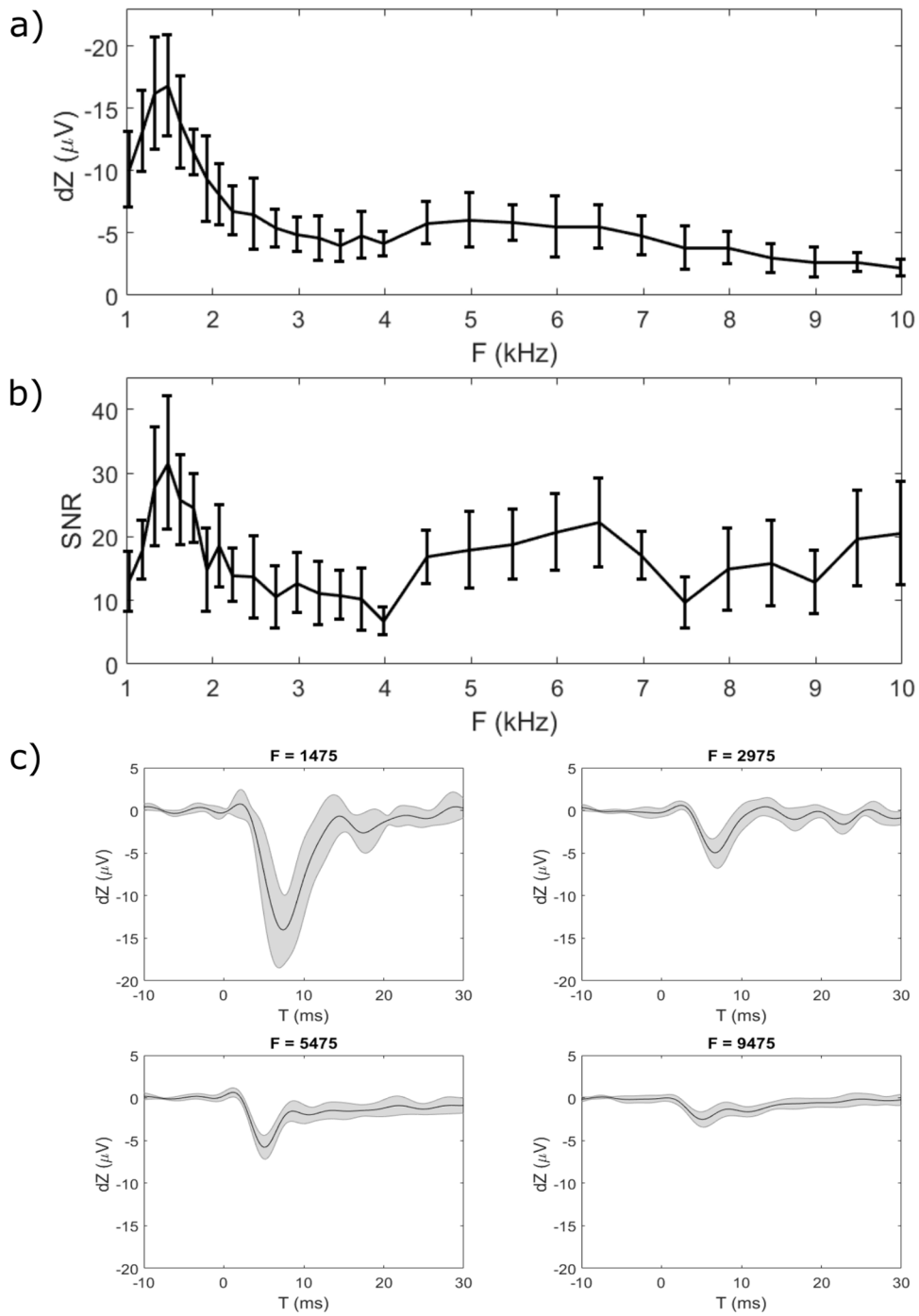

Figure 3. Frequency response of impedance change during somatosensory forepaw stimulation in thalamus. (a) Peak impedance change with varying carrier frequency. (b) SNR with varying carrier frequency. (c) Examples of impedance traces at 1475 Hz, 2975 Hz, 5475 Hz and 9475 Hz. All values are given as (mean ± S.D.).

At 5475 Hz the peak occurred at 5.06 ± 0.3 ms. No frequencies, however, exhibited a significant difference in peak latency compared to the mean across all frequencies ($p < 0.01$).

The largest SNR was 31.6 ± 10 at 1475 Hz (figure 3(b)). Noticeable dips were present at 3975 Hz and 7475 Hz. These can be attributed to increased noise in the system at these frequencies. Frequencies that exhibited a significant SNR lay between 1325 Hz to 1775 Hz in addition to 6475 Hz ($p < 0.01$).

4. Discussion

4.1. Summary of results

In the cortex, the maximum signal and SNR were both observed at 1475 Hz and had values of −15.4 ± 3 μV and 29.5 ± 8 respectively. A similar trend in activity was observed in the thalamus with the largest signal and SNR both being observed at 1475 Hz. These had respective values of −16.9 ± 4 μV and 31.6 ± 10.

4.2. Technical considerations

In order to consistently detect a thalamic impedance change on the depth electrode, current of amplitude 200 μA had to be injected between electrodes on the cortical array. When considering the diameter of the injection electrodes, the local current density exceeded the threshold at which evoked activity by around 3 fold (Liebetanz *et al* 2009, Edwards *et al* 2013, Aristovich *et al* 2015) It is highly likely, therefore, that the neuronal activity just below the injecting electrodes was altered. The injection pairs were chosen such that they were not located near the somatosensory cortex in order to minimise any influence on the feedback circuit between the cortex and thalamus. Thus when characterising the impedance response, it is unlikely that the current would have influenced the overall trend seen in the frequency response in the thalamus. However, if EIT is extended to image more complex paradigms that implicate different regions of the cortex, the influence of this current may be problematic. To mitigate this the use of larger diameter injecting electrodes should be implemented to ensure that the current density is below the level that evokes activity.

4.3. What are the characteristics of the impedance signal across frequency in the cerebral cortex and thalamus?

In the cortex the maximum signal and SNR were both observed at 1475 Hz (figures 2(a) and (b)). The largest response was also observed at this frequency in the thalamus (figures 3(a) and (b)). On qualitative inspection the overall trend across carrier frequency in the signal observed in the cerebral cortex and thalamus was very similar. The signal increased from its value at 1025 Hz to a maximum at 1475 Hz, before decaying away by 3 kHz. At frequencies above this, the signal plateaued in the cortex and remained fairly constant up to 10 kHz. Despite the signal remaining constant, an increase in SNR was observed between 3 kHz and 10 kHz. This could be attributed to lower noise at higher injection frequencies.

In the case of the thalamus, a slight increase in the signal was observed between 4 kHz and 7 kHz (figure 3(a)). For comparison, the largest impedance response in the rat sciatic nerve was observed around 6 kHz (Aristovich *et al* 2016a). It may well be that the signal detected in the thalamus was not only due to VPL neurons but had contributions from spinothalamic fibers that terminate in the VPL (McAlliser and Wells 1981, Burnstein *et al* 1990). While not significant, it is of note that the latency of the peak response at 5475 Hz occurred around 3 ms prior to that observed at 1475 Hz. Further, in the raw impedance trace at 5475 Hz, the thalamic response had a much more distinct negative peak compared to that in the cortex (figures 2(c) and 3(c)).

In general, larger impedance changes were observed in the thalamus, -0.4% in the thalamus compared to -0.13% in the cortex at 1475 Hz. This could be attributed to the recording methods used; thalamic impedance changes were measured directly from the centre of the VPL, whereas cortical impedance changes have been measured from the surface of the cortex, typically 500 μm away from layers III–V (DeFelipe *et al* 2002), which are heavily implicated in somatosensory evoked processing in the cortex (Herkenham 1980, Abbes *et al* 1991).

4.4. How do the impedance responses compare to known electrophysiology and biophysical models?

The peak of the cortical impedance responses occurred 12.7 ms after presentation of the forepaw stimulus. The latency observed is in agreement with cortical evoked potentials occurring 12–17 ms after stimulation under α-chloralose anaesthesia (Koyanagi and Tator 1996, Huttunen *et al* 2008). Angel and Clarke (1975) and Alonso-Calvino *et al* (2016) report evoked potentials from VPL neurons occurring between 5–8 ms after stimulation. These are consistent with the latency of 7.9 ms observed in this study. Previous measurements of cortical impedance changes during evoked activity report amplitudes of 0.007% (Oh *et al* 2011) and 0.1% (Aristovich *et al* 2016b). Their magnitude is consistent with the 0.13% observed here at 1475 Hz in the cortex.

All biophysical models of the impedance change mechanism during fast neural activity developed thus far, predict a monotonic decrease in signal from DC to higher frequencies. The trends in the SNR of the frequency response in both the cortex and thalamus were not consistent with these models. The peak in SNR at 1475 Hz was not only due to decreased noise compared to 1025 Hz, but the magnitude of the signal itself was largest at this frequency.

While both the models developed by Cole (1928) and Liston *et al* (2012) have been extended to characterise cortical tissue, they are based on passive models. The ion channels within the neural membrane are voltage-gated and their resistance depends on the voltage across it. Therefore, unlike the passive model where the ion channels are either in an open or closed state, the externally applied current will influence the nonlinear resistance-voltage dependence of the membrane and its influence will likely vary with frequency. The results obtained in this study suggest that indeed these passive models are insufficient to accurately describe the frequency characteristics of impedance changes in neural tissue.

The non-monotonic nature of the frequency response of impedance changes in the neural tissue indicates that the circuitry underlying its behavior is controlled by an active system that has a resonance centered around 1475 Hz. Individual neurons exhibit an increased response to select frequencies which has been described as a potential mechanism through which neurons differentiate inputs and can be modelled using a parallel RLC

circuit (Hutcheon and Yarom 2000). A possibility is that the peak observed at 1475 Hz is a manifestation of the resonance of the individual neurons. The reported resonant frequency of many neurons, however, is much lower in frequency with the majority exhibiting resonance at frequencies below 300 Hz (Puil *et al* 1986, Hutcheon *et al* 1996, Lea-Carnall *et al* 2016). Due to low SNR and artefacts from the evoked potential at these low frequencies, measurements to corroborate these studies were not obtained. However, the fact that a peak was also observed 1475 Hz indicates that these simple RLC models are not sufficient. The origin of the observed peak could either be due to a harmonic of the original, indicating a non-linear model, or a result of a higher order model that allows for multiple resonance peaks.

The model developed by Tarotin *et al* (2017) takes into account both the passive and active properties of neuronal membranes. It has so far, however, only been extended to simulate the frequency characteristics of interacting unmyelinated nerve fibers and this may explain its shortcoming in adequately describing the observed response. By extending this to model interacting myelinated and unmyelinated fibers it may elucidate the origin of the peak change observed at 1475 Hz. We hope that this dataset can help inform and guide future models attempting to describe the mechanism occurring during impedance measurements of fast neural activity in the brain.

4.5. What are the implications for fast neural EIT applications in the brain?

4.5.1. Multi-frequency parallel EIT

Above frequencies of 3 kHz, the impedance response observed remained fairly constant in magnitude and shape. The recommendation for multi-frequency parallel EIT applications would thus be to take advantage of this uniformity in the signal and choose carrier frequencies in this range. Above 3 kHz the SNR actually increased with frequency and so choosing injection frequencies as high as possible would be advantageous.

4.5.2. Deep imaging

In order to conduct deep imaging the recommendation from this work would be to use a carrier frequency of 1475 Hz. At this frequency the local impedance change occurring in the VPL had an amplitude of 0.4%. Simulations undertaken by Aristovich *et al* (2016b) indicated that a 1% conductivity change could be imaged throughout the rat brain with an accuracy of 500 μm. While the magnitude of the response observed is half that simulated, through optimisation of the protocol and by increasing the number of averages, it is not inconceivable that EIT could be used to image this activity from the cortex.

Acknowledgments

This work was supported by DARPA grant N66001-16-2-4066, Blackrock Microsystems and the EPSRC (EP/M506448/1).

ORCID iDs

Mayo Faulkner https://orcid.org/0000-0001-5427-0282
James Avery https://orcid.org/0000-0002-4015-1802

References

Abbes S, Louvel J, Lamarche M and Pumain R 1991 Laminar analysis of the origin of the various components of evoked potentials in slices of rat sensorimotor cortex *Electroencephalogr. Clin. Neurophysiol. Evoked Potentials* **80** 310–20

Aguilar J, Morales-Botello M and Foffani G 2008 Tactile responses of hindpaw, forepaw and whisker neurons in the thalamic ventrobasal complex of anesthetized rats *Eur. J. Neurosci.* **27** 378–87

Alessandrini G and Scapin A 2017 Depth dependent resolution in electrical impedance tomography *J. Inverse lll-Posed Problems* **25** 391–402

Alonso-Calvino E, Martinez-Camero I, Fernandez-Lopez E, Humanes-Valera D, Foffani G and Aguilar J 2016 Increased responses in the somatosensory thalamus immediately after spinal cord injury *Neurobiol. Dis.* **87** 39–49

Angel A and Clarke K 1975 An analysis of the representation of the forelimb in the ventrobasal thalamic complex of the albino rat *J. Physiol.* **249** 399–423

Aristovich K Y, Dos Santos G S and Holder D S 2015 Investigation of potential artefactual changes in measurements of impedance changes during evoked activity: implications to electrical impedance tomography of brain function *Physiol. Meas.* **36** 1245

Aristovich K, Blochet C, Avery J, Donega M and Holder D 2016a EIT of evoked and spontaneous activity in peripheral nerve *Proc. 17th Int. Conf. on Electrical Impedance Tomography*

Aristovich K Y, Packham B C, Koo H, dos Santos G S, McEvoy A and Holder D S 2016b Imaging fast electrical activity in the brain with electrical impedance tomography *NeuroImage* **124** 204–13

Avery J, Dowrick T, Faulkner M, Goren N and Holder D 2017 A versatile and reproducible multi-frequency electrical impedance tomography system *Sensors* **17** 280

Burnstein R, Dado R and Giesler G 1990 The cells of origin of the spinothalamic tract of the rat: a quantitative re-examination *Brain Res.* **511** 329–37

Cole K S 1928 Electric impedance of suspensions of spheres *J. Gen. Physiol.* **12** 29–36

Cole S and Curtis H 1939 Electrical impedane of the squid giant axon during activity *J. Gen. Physiol.* **22** 649–70

DeFelipe J, Alonso-Nanclares L and Arellano J I 2002 Microstructure of the neocortex: comparative aspects *J. Neurocytology* **31** 299–316
Dowrick T, Dos Santos G S, Vongerichten A and Holder D 2015 Parallel, multi frequency eit measurement, suitable for recording impedance changes during epilepsy *J. Electr. Bioimpedance* **6** 37–43
Edwards D, Cortes M, Datta A, Minhas P, Wassermann E M and Bikson M 2013 Physiological and modeling evidence for focal transcranial electrical brain stimulation in humans: a basis for high-definition TDCS *Neuroimage* **74** 266–75
Gilad O and Holder D S 2009 Impedance changes recorded with scalp electrodes during visual evoked responses: implications for electrical impedance tomography of fast neural activity *Neuroimage* **47** 514–22
Herkenham M 1980 Laminar organization of thalamic projections to the rat neocortex *Science* **207** 532–5
Hodgkin A L and Huxley A F 1952 A quantitative description of membrane current and its application to conduction and excitation in nerve *J. Physiol.* **117** 500–44
Holder D, Rao A and Hanquan Y 1996 Imaging of physiologically evoked responses by electrical impedance tomography with cortical electrodes in the anaesthetized rabbit *Physiol. Meas.* **17** A179
Hutcheon B and Yarom Y 2000 Resonance, oscillation and the intrinsic frequency preferences of neurons *Trends Neurosci.* **23** 216–22
Hutcheon B, Miura R M and Puil E 1996 Models of subthreshold membrane resonance in neocortical neurons *J. Neurophysiol.* **76** 698–714
Huttunen J K, Gröhn O and Penttonen M 2008 Coupling between simultaneously recorded bold response and neuronal activity in the rat somatosensory cortex *Neuroimage* **39** 775–85
Klivington K A and Galambos R 1967 Resistance shifts accompanying the evoked cortical response in the cat *Science* **157** 211–3
Koyanagi I and Tator C H 1996 The effects of cortical stimulation, anesthesia and recording site on somatosensory evoked potentials in the rat *Electroencephalogr. Clin. Neurophysiol. Electromyogr. Motor Control* **101** 534–42
Lea-Carnall C A, Montemurro M A, Trujillo-Barreto N J, Parkes L M and El-Deredy W 2016 Cortical resonance frequencies emerge from network size and connectivity *PLoS Comput. Biol.* **12** e1004740
Liebetanz D, Koch R, Mayenfels S, König F, Paulus W and Nitsche M A 2009 Safety limits of cathodal transcranial direct current stimulation in rats *Clin. Neurophysiol.* **120** 1161–7
Liston A, Bayford R and Holder D 2012 A cable theory based biophysical model of resistance change in crab peripheral nerve and human cerebral cortex during neuronal depolarisation: implications for electrical impedance tomography of fast neural activity in the brain *Med. Biol. Eng. Comput.* **50** 425–37
McAlliser J and Wells J 1981 The structural organization of the ventral posterolateral nucleus in the rat *J. Comparative Neurol.* **197** 271–301
Oh T, Gilad O, Ghosh A, Schuettler M and Holder D S 2011 A novel method for recording neuronal depolarization with recording at 125–825 Hz: implications for imaging fast neural activity in the brain with electrical impedance tomography *Med. Biol. Eng. Comput.* **49** 593–604
Paxinos G 2014 *Somatosensory System* (New York: Academic)
Puil E, Gimbarzevsky B and Miura R 1986 Quantification of membrane properties of trigeminal root ganglion neurons in guinea pigs *J. Neurophysiol.* **55** 995–1016
Tarotin I, Aristovich K and Holder D 2017 Model of impedance changes in unmyelinated fibres *Proc. 18th Int. Conf. on Biomedical Applications of Electrical Impedance Tomography*
Velluti R, Klivington K and Galambos R 1968 Evoked resistance shifts in subcortical nuclei *Curr. Mod. Biol.* **2** 78–80
Vongerichten A 2014 Imaging physiological and pathological activity in the brain using electrical impedance tomography *PhD Thesis* University College London
Vongerichten A N, dos Santos G S, Aristovich K, Avery J, McEvoy A, Walker M and Holder D S 2016 Characterisation and imaging of cortical impedance changes during interictal and ictal activity in the anaesthetised rat *NeuroImage* **124** 813–23